Titanium-Immobilized Layered HUS-7 Silicate as a Catalyst for Photocatalytic CO$_2$ Reduction

Rudolf Ricka,[a, b] Tareq W. M. Amen,[c] Nao Tsunoji,[c] Martin Reli,[a] Miroslava Filip Edelmannová,[a] Martin Kormunda,[d] Michal Ritz,[b] and Kamila Kočí*[a, e]

Utilizing photocatalytic CO$_2$ reduction presents a promising avenue for combating climate change and curbing greenhouse gas emissions. However, maximizing its potential hinges on the development of materials that not only enhance efficiency but also ensure process stability. Here, we introduce Hiroshima University Silicate-7 (HUS-7) with immobilized Ti species as a standout contender. Our study demonstrates the remarkable photocatalytic activity of HUS-7 in CO$_2$ reduction, yielding substantially higher carbonaceous product yields compared to conventional titanium-based catalysts TS-1 and P25. Through thorough characterization, we elucidate that their boosted photocatalytic performance is attributed to the incorporation of isolated Ti species within the silica-based precursor, serving as potent photoinduced active sites. Moreover, our findings underscore the crucial role of the Ligand-to-Metal Charge Transfer (LMCT) process in facilitating the photoactivation of CO$_2$ molecules, shedding new light on key mechanisms underlying photocatalytic CO$_2$ reduction.

1. Introduction

Global warming of the planet associated with climate change represents the major environmental issue of the modern era. The rapid growth of the world's population and industrialization, beginning with the Industrial Revolution in the 19th century, have led to massive consumption of fossil fuels and thus to the simultaneous release of greenhouse gases, mainly CO$_2$, into the atmosphere.[1–5] In view of these facts, it is clear that new efficient strategies for CO$_2$ utilization must be designed to mitigate its negative impact on the atmosphere.

Fortunately, the photocatalytic reduction of CO$_2$ represents a promising approach to convert CO$_2$ molecules into other useful chemical compounds (such as CH$_4$ or CH$_3$OH).[6] Although much progress has been achieved in the field of photocatalytic CO$_2$ reduction, as evidenced by the increasing number of publications published in recent decades, the practical application of this technology is very limited due to the low level of CO$_2$ conversion. Since CO$_2$ is a very stable molecule (bond energy of C=O: $\triangle H = 750–800$ kJ mol^{-1}), a large amount of energy must be supplied to the photocatalytic system to disrupt the C=O bonds present in the CO$_2$ molecule.[7–9] Given these facts, it can be summarized that the photocatalytic reduction of CO$_2$ represents a very complicated process, and to overcome the mentioned drawbacks and thus achieve an increase in the efficiency of the photocatalytic CO$_2$ reduction, it is necessary not only to develop new photocatalytic technologies, but also to design and synthesize efficient photocatalytically active materials.[10,11]

The most investigated nanomaterial in photocatalysis is titanium dioxide (TiO$_2$). The application of this photocatalyst offers many advantages, such as its high chemical and thermal stability, high reactivity, corrosion resistance, low cost, and high abundance.[12–14] Although TiO$_2$ is considered to be the most promising photocatalyst, the high recombination rate of photogenerated pairs and the large band gap energy (E$_g$ = 3.2 eV) severely limit its photocatalytic properties and consequently its applicability for photocatalytic reactions.[15] In light of these assertions, it is essential to persist in developing new photocatalytically active materials or enhancing the photocatalytic properties of existing ones. This effort represents one of the crucial steps in enhancing the efficiency of the photocatalytic CO$_2$ reduction.

Silica-based materials with tetrahedrally coordinated transition metals, such as Ti, Cu, and V, immobilized within the silica framework, demonstrate potential as promising candidates applicable not only in various catalytic but also in photocatalytic reactions. The unique catalytic and photocatalytic properties of these environmentally friendly materials primarily stem from the functional features of active transition metal active centers. Furthermore, their ligand to metal charge

[a] Institute of Environmental Technology, CEET, VŠB-Technical University of Ostrava, Poruba, Czech Republic

[b] Faculty of Materials Science and Technology, VŠB-Technical University of Ostrava, Poruba, Czech Republic

[c] Department of Applied Chemistry, Graduate School of Advanced Science and Engineering, Hiroshima University, Higashihiroshima, Higashi-Hiroshima, Japan

[d] Department of Physics, Faculty of Science, J. E. Purkyně University, Ústí and Labem, Czech Republic

[e] Department of Physics and Materials Engineering, Faculty of Technology, Tomas Bata University in Zlín, Zlín, Czech Republic

Correspondence: Kamila Kočí, Institute of Environmental Technology, CEET, VŠB-Technical University of Ostrava, 17. listopadu 2172/15, Ostrava-Poruba 708 00, Czech Republic.
Email: kamila.koci@vsb.cz

transfer (LMCT) property significantly contributes to their distinctive characteristics.[16–21]

In this work, layered silicate photocatalysts with immobilized titanium complex (Ti-HUS) were prepared. Samples were synthesized by the grafting of titanium (IV) acetylacetonate (source of titanium atoms) onto the layered silicate HUS-7 precursor.[17,22,23] Although titanosilicate typically limits the content of titanium incorporated (around 2 wt.%), this material overcomes the compositional limitation. During the grafting process of this layered titanosilicate material, abundant connection points arranged by the crystallographic order (surface silanol group on the silicate layer) cause successful immobilization of a large number of isolated titanium species with uniform coordination state.

Here, the layered Ti-HUS photocatalysts, featuring varying amounts of immobilized Ti species on the layered silicate HUS-7 precursor, were synthesized. Successful modulation of Ti species was achieved through acid treatment. The photocatalysts were then thoroughly characterized using various analytical techniques to obtain a comprehensive understanding of their physicochemical properties. The measured analytical data were further correlated with the results from the photocatalytic reduction of CO_2. These correlations were conducted in the presence of the synthesized layered Ti-HUS-based photocatalysts. The aim was to clarify how individual physico-chemical properties influence the resulting photocatalytic performance of the these photocatalyst samples during the photocatalytic CO_2 reduction. Finally, the photocatalytic efficiency of the investigated layered Ti-HUS photocatalysts was compared with the photocatalytic performances of the reference samples of the commercial TiO_2 photocatalyst P25 and TS-1.

Experimental Section

Synthesis of Ti-HUS Photocatalyst

The Ti-HUS photocatalyst was synthesized by the grafting of the Ti-complex on the ion-exchanged layered silicate precursor according to the previous method.[17,22,23] The preparation was carried out in the following steps: first, a mixture of hexadecyltrimethylammonium (C16TMA)-exchanged layered silicate C_{16}TMA HUS-7, titanium (IV) acetylacetonate, Ti(acac)$_4$, and toluene was stirred for 24 hours. Subsequently, the mixture was stirred for another 24 hours, but with the addition of dodecylbenzenesulfonic acid ($C_{12}BSO_3H$). After stirring, the obtained solid was separated by filtration, washed with toluene, and finally dried at 70 °C overnight in a drying oven.

Synthesis of HCl/Ti-HUS Photocatalyst

The HCl/Ti-HUS photocatalyst was synthesized by mixing 1.2 g of the prepared Ti-HUS photocatalyst with 50 ml of aqueous HCl solution. The prepared suspension was stirred for 24 hours. After stirring, the solid obtained was separated by centrifugation, washed with deionized water, and dried at 70 °C overnight. The same procedure was repeated three times with three pre-selected concentrations of aqueous HCl solutions (0.1, 3.0, and 6.0 mol dm^{-3}) to obtain three different HCl/Ti-HUS-based photocatalysts. An image of the prepared photocatalysts after chlorination treatment is presented in Figure S1 in the Supplementary Materials. Overall,

four Ti-HUS-based photocatalyst samples were synthesized (Ti-HUS, 0.1 M_HCl/Ti-HUS, 3.0 M_HCl/Ti-HUS, 6.0 M_HCl/Ti-HUS). Finally, their photocatalytic activity for CO_2 reduction was compared with the samples of Titanium Silicate material TS-1 and commercial TiO_2 photocatalyst P25.

Photocatalytic Reduction of CO_2

Photocatalytic CO_2 reduction experiments were performed in a batch photoreactor (stainless steel, volume 357 cm^3, Figure S2). A detailed description of the photocatalytic experiment is provided in the Supplementary Materials.

Characterization

The investigated photocatalyst samples were thoroughly characterized by X-ray diffraction analysis (XRD), X-ray photoelectron spectroscopy (XPS), scanning electron microscopy equipped with energy dispersive spectroscopy (SEM-EDX), Fourier-transform infrared spectroscopy (FTIR), Raman spectroscopy, N_2-adsorption, and Ultraviolet-visible diffuse reflectance spectroscopy (UV-Vis/DRS). A description of the applied characterization methods is included in the Supplementary Materials.

Calculation of Interlayer Spacing of Ti-HUS-Based Photocatalyst Samples

The interlayer spacing of the crystal layers of the investigated Ti-HUS layered photocatalysts was determined by Bragg's equation (Eq. 1.):[24]

$$n \cdot \lambda = 2d \cdot \sin(\theta) \tag{1}$$

where n (–) is the diffraction order, λ (nm) is the wavelength of X-ray irradiation, d (nm) is the interlayer spacing and $\sin(\theta)$ (°) is the glancing angle.

Calculation of Selectivity for the CO_2 Reduction Process

The percentage selectivity for the photocatalytic CO_2 reduction over the investigated photocatalyst samples was calculated using Equation 2:[18]

$$\text{Selectivity for } CO_2 \text{ reduction} = \frac{[2r(CO) + 8r(CH_4)]}{[2r(CO) + 8r(CH_4) + 2r(H_2)]} \cdot 100\% \tag{2}$$

2. Results and Discussion

2.1. Characterization of the Investigated Photocatalysts

The synthesized Ti-HUS-based photocatalyst samples were first thoroughly characterized using a variety of analytical techniques to obtain more details about their physicochemical properties. Subsequently, the provided data were correlated with the results of the photocatalytic reduction of CO_2 to explain the differences in the photocatalytic activity of individual samples and to verify the suitability of applying the Ti-HUS-based photocatalysts for the photocatalytic reduction of CO_2 reaction.

ChemSusChem

Research Article
doi.org/10.1002/cssc.202400434

Chemistry Europe
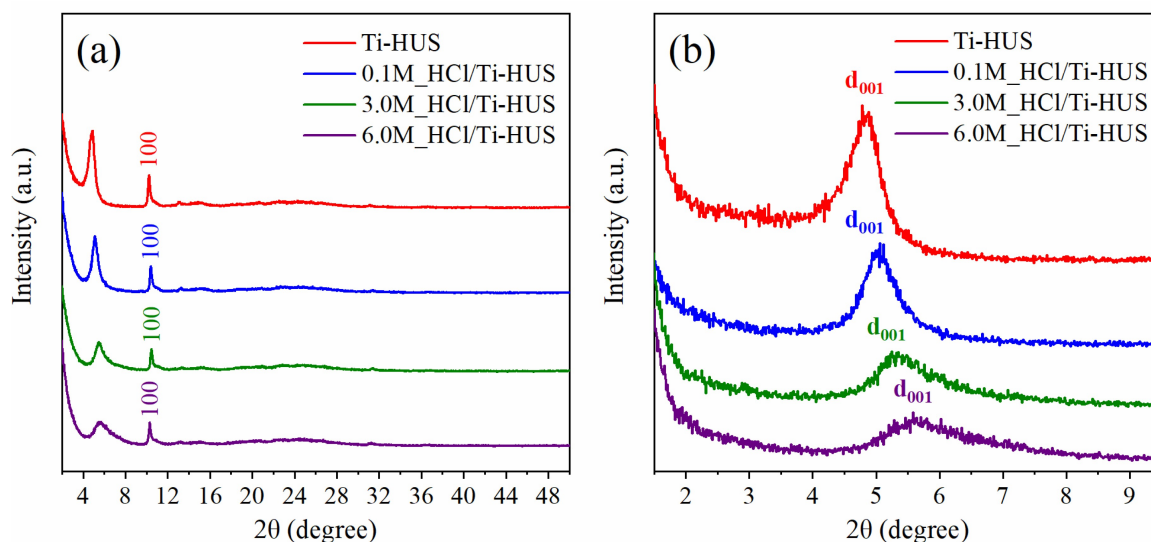European Chemical
Societies Publishing

Figure 1. a) Wide-angle and b) low-angle XRD patterns of the synthesized Ti-HUS-based materials before and after hydrochloric acid treatment.

The crystalline structure of the synthesized samples was analyzed using powder XRD analysis. Based on the XRD patterns obtained, as depicted in Figure 1 a, it can be stated that the silicate layer of the HUS-7 was preserved in the structure of the synthesized Ti-HUS-based photocatalyst samples, even though the samples were subjected to the incorporation of titanium atoms and subsequent acid treatment.[22] This fact is demonstrated by the presence of diffraction peaks at $2\theta = 10.5°$, corresponding to the in-plane (100) of the silicate layer of HUS-7. As shown in the data in Table 1, the XRD analysis also revealed a gradual drop in the interlayer spacing (d_{001}) of Ti-HUS-based samples after acid treatment (0.1 M_HCl/Ti-HUS, 3.0 M_HCl/Ti-HUS, 6.0 M_HCl/Ti-HUS), which can be attributed to the release of interlayer molecules (such as a titanium and organic ligands).[22] This observation is consistent with a gradual decrease in the intensity of the diffraction peaks within the 2θ range between 4.78 and 5.59, as illustrated in Figure 1b.

In order to obtain details about the surface chemical composition of the synthesized layered photocatalyst samples, XPS analysis was performed. Based on the XPS results, it can be summarized that Si, O, and C are predominantly present on the surface of Ti-HUS-based photocatalysts, while Ti is present in low concentrations. A table presenting the surface chemical composition of the Ti-HUS samples in relative percentages is provided in the Supplementary Materials (Table S1).

XPS revealed that titanium species were successfully immobilized on the surface of the silicate layer precursor. This fact is supported by the presence of Ti $2p_{1/2}$ and Ti $2p_{3/2}$ peaks, corresponding to Ti(IV).[25] The presence of these peaks is evident from the measured Ti 2p spectra of the Ti-HUS-based samples shown in Figure 2, where a spin-split doublet is visible for Ti $2p_{3/2}$ at 459.2 ± 0.2 eV with $dE = 5.8$ eV to Ti $2p_{1/2}$, closely approximating the Ti(IV) value reported by Biesinger et al..[26] There is no evidence of substoichimetric Ti oxides at lower binding energies.[26] The shift can be caused by non-homogeneous sample charge due to the limited conductivity of the powder grains in direct contacts, and the sam effect is responsible for an increase in full with half maxims.

According to the literature,[27] the efficiency of the photocatalytic reduction of CO_2 can be significantly influenced by the existence of oxygen within the surface hydroxyl groups (—OH). To detect and quantify these groups, the XPS O 1 s spectra of the synthesized Ti-HUS-based were measured and analysed. As shown in Figure 3, all photocatalyst samples exhibit the presence of a peak with a maximum at 532.4 eV, which can be attributed to lattice oxygen (O lattice) in silica structure[28] rather than the expected 529.9 eV in TiO_2.[26] Since the Ti content is low compared to other metals (such as Si), it is complicated to accurately detect Ti—O in the O 1 s spectra shown in Figure 3. Furthermore, in the XPS O 1 s spectra of the untreated Ti-HUS and the treated 0.1 M_HCl/Ti-HUS samples, additional peaks were identified with maxima in the range of binding energy values 534.0–534.7 eV, corresponding to the typical hydroxyl groups.

Subsequent quantification of the XPS results demonstrated the majority presence of lattice oxygen (Table 2). The highest abundance of hydroxyl groups was determined on the surface of the unmodified Ti-HUS sample. Based on the obtained data, it is also possible to indicate that the quantity of hydroxyl groups decreases with gradually with an increase in the concentration of HCl used during acid treatment.
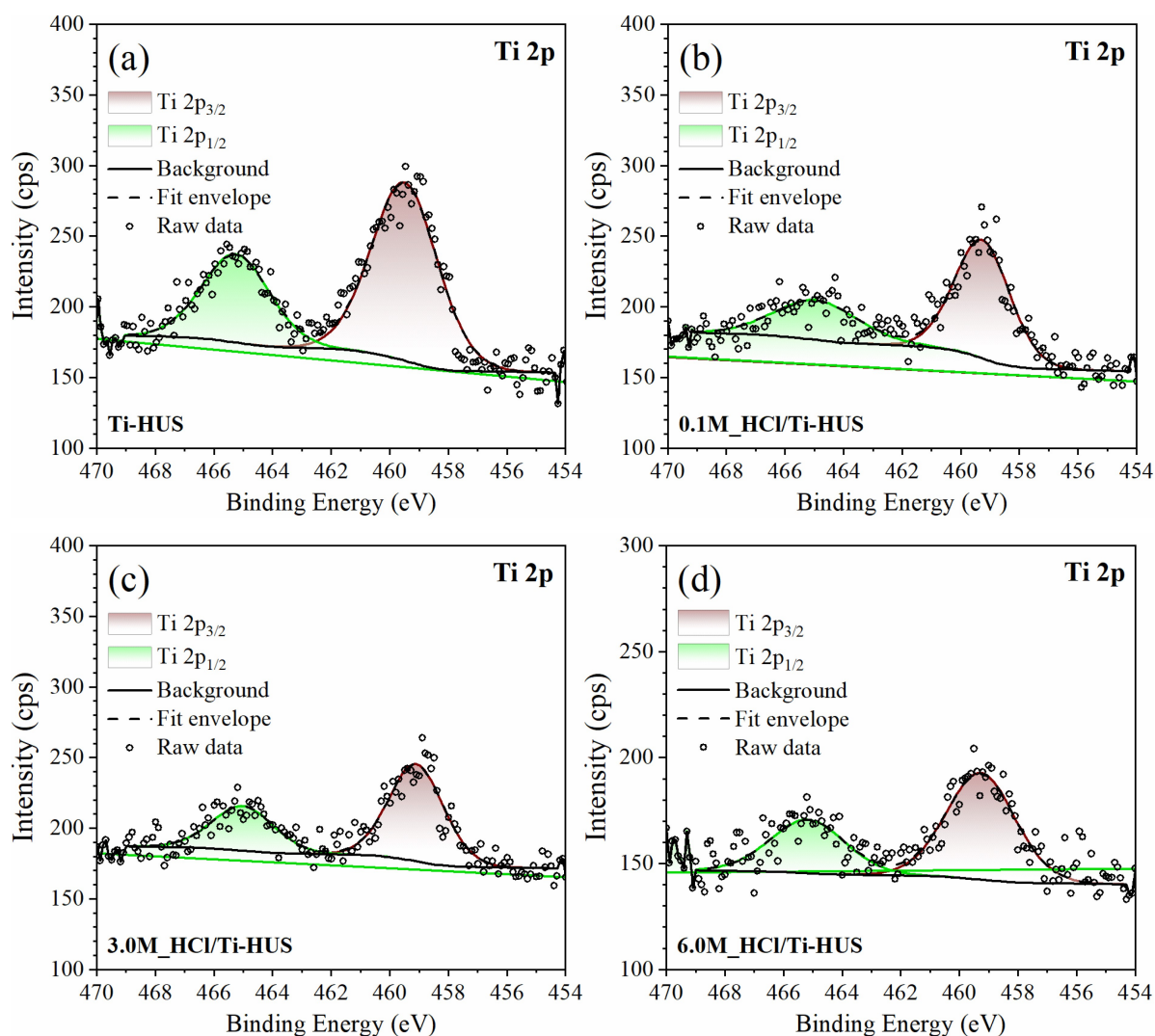
Table 1. Calculated values of the interlayer spacings of the investigated Ti-HUS-based photocatalysts.

Sample	d_{001} (nm) [a]
Ti-HUS	1.82
0.1 M_HCl/Ti-HUS	1.74
3.0 M_HCl/Ti-HUS	1.61
6.0 M_HCl/ Ti-HUS	1.62

[a] Calculated using Bragg's equation (Eq. 1.).

ChemSusChem

Research Article
doi.org/10.1002/cssc.202400434

**Chemistry
Europe**
European Chemical
Societies Publishing

Figure 2. Ti 2p XPS spectra of a) Ti-HUS, b) 0.1 M_HCl/Ti-HUS, c) 3.0 M_HCl/Ti-HUS, and d) 6.0 M_HCl/Ti-HUS.

Table 2. Quantitative analysis of lattice oxygen and hydroxyl groups detected on the surface of the prepared Ti-HUS-based materials.

Sample	O 1s	
	O lattice (at. %)	−OH (at. %)
Ti-HUS	33	6
0.1 M_HCl/Ti-HUS	38	3
3.0 M_HCl/Ti-HUS	40	0
6.0 M_HCl/Ti-HUS	37	0

Since organic compounds were used in the synthesis of the investigated Ti-HUS-based layered photocatalyst samples, it was necessary to investigate the presence of hydrocarbons that could potentially affect the photocatalytic reduction of CO_2 process. This information was provided by both the XPS and FTIR results. As shown in Table 3, the XPS analysis demonstrated the presence of C–C, C–O, and C=O bonds on the surface of the synthesized samples. The relative percentages of the mentioned C–C, C–O, and C=O bonds are provided in Table 3.

The presence of hydrocarbons in the structure of the investigated Ti-HUS-based materials was also demonstrated by FTIR analysis. This fact is evident from the measured FTIR spectra in Figure 4, indicating the presence of aliphatic C–H groups corresponding to peaks in the ranges of vavenumbers 1351–1468 and 2851–2961 cm^{M-1}.[29–31] Additionally, the bonds observed at in the range of 3415–3438 cm^{-1} correspond to the presence of hydroxyl groups from adsorbed molecules of H_2O.[32,33] Furthermore, the measured peaks (SiO_4) LO, (SiO_4) TO, and (SiO_4) at 1183–1184, 1074–1076, and 802–810 cm^{-1} in the FTIR spectra can be attributed to the presence of a silica-based network.[34] FTIR analysis also revealed the formation of a Si–O–Ti bond, confirmed by a peaks at 941–943 cm^{-1}.[35,36] The presence of the Si–O–Ti bond is associated with the successful immobilization of isolated Ti centers into the structure of the silicate layer precursor.

A detailed description of the detected bonds is given in Table 4.

Based on EDX and XPS analyses, it was found that the acid treatment of Ti-HUS resulted in the depletion of titanium
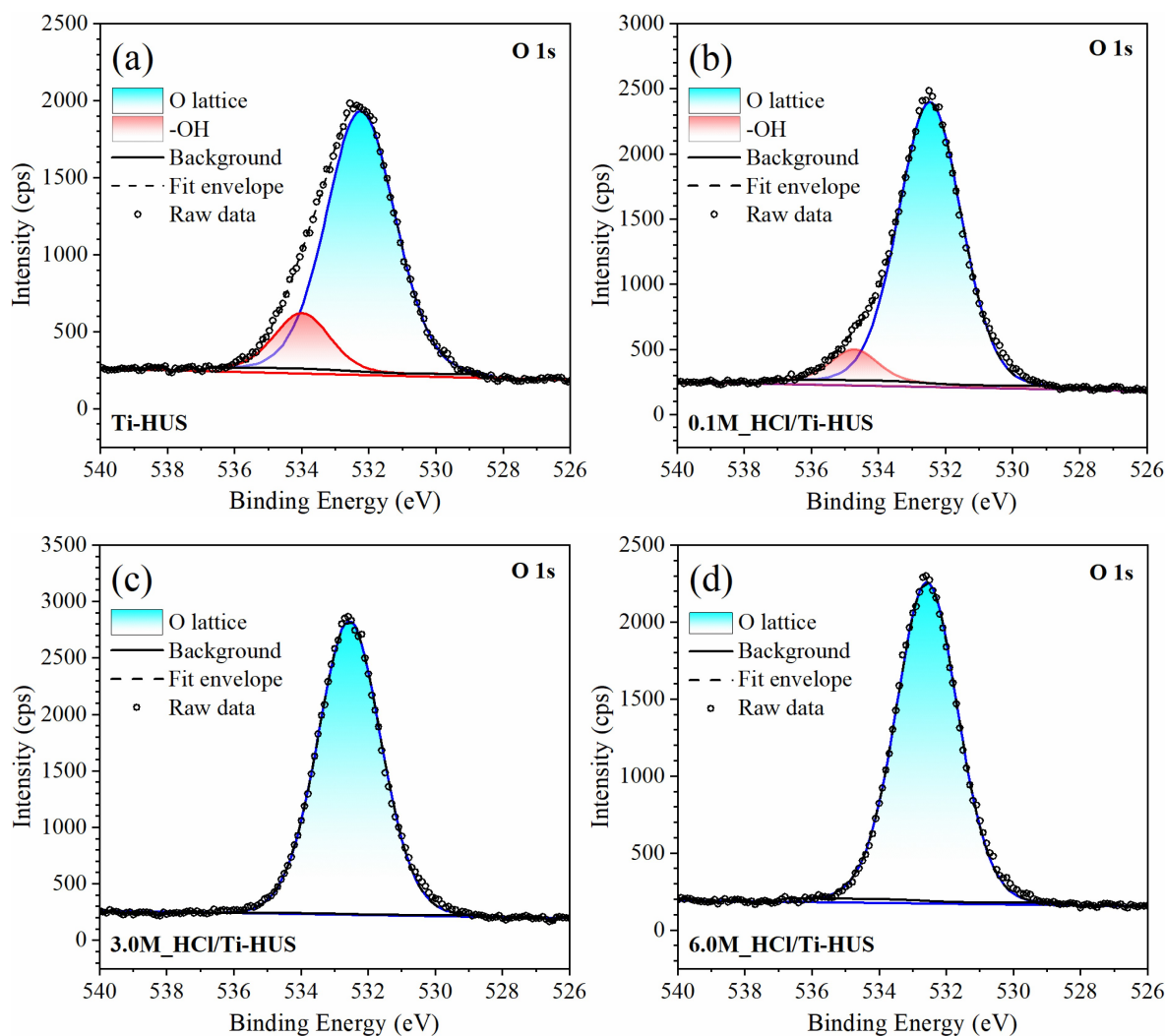
Figure 3. XPS and O 1s spectra of a) Ti-HUS, b) 0.1 M_HCl/Ti-HUS, c) 3.0 M_HCl/Ti-HUS, and d) 6.0 M_HCl/Ti-HUS.

Table 3. Representation of C–C, C–O, and C=O bonds in relative percentages.

Sample	C 1 s [a]		
	C–C (%)	C–O (%)	C=O (%)
Ti-HUS	41	49	9
0.1 M_HCl/Ti-HUS	58	37	5
3.0 M_HCl/Ti-HUS	69	30	1
6.0 M_HCl/Ti-HUS	71	28	1
[a] Determined by XPS analysis.			

Figure 4. FTIR spectra of the investigated samples. A detailed description of the detected bonds is given in Table 4.

species, as evidenced by the increasing Si/Ti ratios shown in Table 5. Additionally, the N_2-adsorption technique, which provided data on the textural parameters, demonstrated that acid treatment of the Ti-HUS photocatalyst resulted in a slight decrease in both surface area (S_{BET}) and total volume values (V_{total}, Table 6).

As shown in Figure S3, the morphology of the synthesized photocatalyst samples was studied by scanning electron micro-
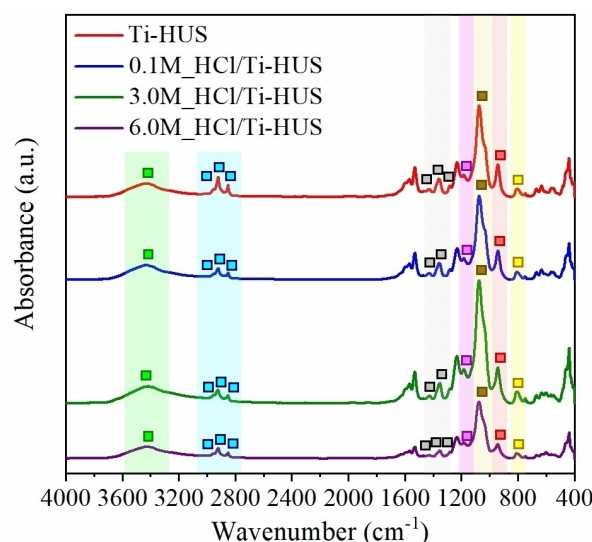
ChemSusChem

Research Article
doi.org/10.1002/cssc.202400434

Chemistry
Europe
European Chemical
Societies Publishing

Table 4. Types of detected bonds, their positions as a function of wavenumbers, and their designation in FTIR spectra, as depicted in Figure 4.

Type of bond	Range of wavenumbers (cm^{-1})	Designation of the detected bond
(SiO_4)	802–810	
Si–O-Ti	941–943	
(SiO_4) TO	1074–1076	
(SiO_4) LO	1183–1184	
C–H aliphatic bending group	1351–1468	
C–H stretching aliphatic group	2851–2961	
OH	3415–3438	

Table 5. Si/Ti ratios of the synthesized photocatalyst samples.

Sample	Si/Ti [a]	Si/Ti [b]
Ti-HUS	9.08	14.80
0.1 M_HCl/Ti-HUS	9.84	27.88
3.0 M_HCl/Ti-HUS	12.30	41.17
6.0 M_HCl/Ti-HUS	15.50	37.43

[a] Determined by EDX techniques. [b] Calculated from measured XPS data.

Table 6. Specific surface areas (S_{BET}) and total pore volumes (V_{total}) of the synthesized Ti-HUS-based photocatalysts.

Sample	S_{BET} ($m^2\ g^{-1}$)	V_{total} ($cm^3\ g^{-1}$)
Ti-HUS	14.3	0.098
0.1 M_HCl/Ti-HUS	14.0	0.095
3.0 M_HCl/Ti-HUS	11.8	0.040
6.0 M_HCl/Ti-HUS	13.2	0.037

scopy (SEM). The SEM images of all material samples before and after acid treatment show a layered morphological structure composed of disc-shaped plates. The size of the observed plates ranges from approximately 2 to 3 μm. Based on these facts, it can be concluded that the acid treatment had no significant effect on the morphology of the investigated samples, as there was no significant change in the size and shape of the observed plates.

The light absorption ability is one of the crucial parameters in the field of photocatalysis. To obtain details on this parameter, the synthesized Ti-HUS photocatalyst samples were analyzed using UV-Vis diffuse reflectance spectroscopy. The UV-Vis DRS analysis performed demonstrated the high light absorption ability of the synthesized layered photocatalyst samples in the UV region of the light spectrum (Figure S4). This

observation corresponds to an increase in absorbance in the wavelength range between 200 and 400 nm. Furthermore, the increase in absorbance within the wavelength range from approximately 280 to 430 nm is associated with the π-π* transition of the acetylacetonate ligand.[37,38] In addition, within the wavelengths from 200 to 230 nm, a slight rise is observable, which can be attributed to LMCT by the immobilized tetrahedrally coordinated Ti^{4+} species.[39,40] Their successful immobilization was demonstrated by Raman spectroscopy, whose spectra (Figure 5a–b) show bands with maxima at 943–946 (green marks) and 1121–1124 cm^{-1} (blue marks). These vibrations are characteristic for the presence of tetrahedrally coordinated Ti^{4+} species.[41–43] The presence of these species was also confirmed by a high-energy shift in the Ti $2p_{3/2}$ peak of the synthesized samples, showing significant shifts to higher binding energy values, ranging from 459.2 to 459.6 eV (Figure 5c–f), compared to those of octahedrally coordinated Ti^{4+} species. These exhibit a maximum of the Ti $2p_{3/2}$ peak in the range of approximately 458.5 to 458.6 eV.[44–46] The prepared Ti-HUS-based samples exhibit a slight extension into the visible region of the light spectrum, which is consistent with high light absorption in the range of wavelengths from 400 to 450 nm.

2.2. Photocatalytic Performance of the Investigated Photocatalysts

The photocatalytic efficiency of the synthesized Ti-HUS-based photocatalyst samples, containing different amounts of Ti species, was evaluated by a 7-hour photocatalytic CO_2 reduction process, using a UVC lamp ($\lambda_{max} = 254$ nm) as the light source. The yields of the detected products (CO, CH_4, and H_2) obtained by analyzing the gaseous phase samples taken at pre-selected time intervals (0, 2, 4, 6, and 7 hours) during the photocatalytic reduction of CO_2, are presented in Figure S5.

ChemSusChem

Research Article
doi.org/10.1002/cssc.202400434

Chemistry Europe
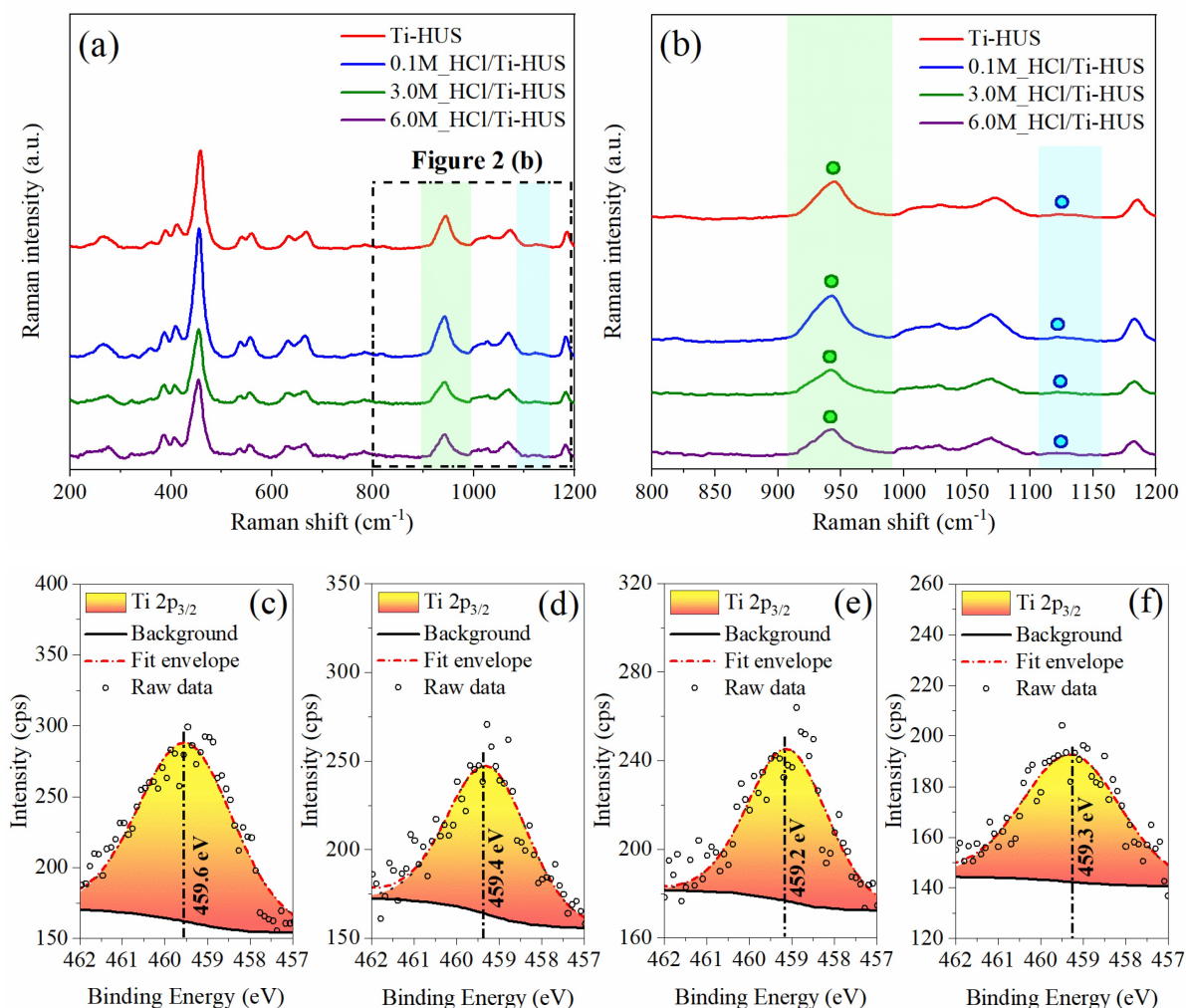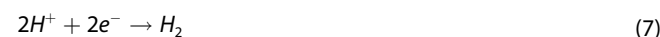European Chemical
Societies Publishing

Figure 5. Raman spectra of the investigated samples (a), zoom of the Raman spectra with the marked bands and marks indicating the presence of immobilized tetrahedrally Ti^{4+} species (b), the Ti 2p XPS spectra of Ti-HUS sample show the Ti $2p_{3/2}$ peak with a maximum at 459.6 eV (c), the Ti 2p XPS spectra of 0.1 M_HCl/Ti-HUS sample exhibit the Ti $2p_{3/2}$ peak with a maximum at 459.4 eV (d), the Ti 2p XPS spectra of 3.0 M_HCl/Ti-HUS sample display the Ti $2p_{3/2}$ peak with a maximum at 459.2 eV (e), and the Ti 2p XPS spectra of 6.0 M_HCl/Ti-HUS sample depict the Ti $2p_{3/2}$ peak with a maximum at 459.3 eV (f).

Based on the yields of the detected gaseous products (CO, CH_4, H_2) after 7-hour exposure to UVC light, as shown in Figure 6, it is evident that the synthesized Ti-HUS-based samples exhibit significantly higher photocatalytic activity for the CO_2 reduction compared to the reference samples of the titanosilicate TS-1 and the commercial TiO_2 P25, which serves as a benchmark in photocatalysis. Their superior photocatalytic efficiency for a CO_2 reduction is reflected primarily in the CO and CH_4 yields (Figure 6a–b), which represent one of the main products of the photocatalytic reduction of CO_2 process. The mechanism of CO_2 conversion to CO and CH_4 during the photocatalytic CO_2 reduction can be described by Equations 3. and 4.[47,48]

$$CO_2 + 2H^+ + 2e^- \rightarrow CO + H_2O \quad (3)$$

$$CO_2 + 8H^+ + 8e^- \rightarrow CH_4 + 2H_2O \quad (4)$$
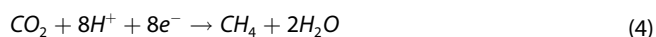
As shown in Figure 6 c, it is apparent that the photocatalytic reduction of CO_2 reaction is not only linked to the formation of CO and CH_4, but also with the evolution of H_2. The generation of hydrogen is related to the water splitting reaction, which competes with the photocatalytic CO_2 reduction.[27] It should be noted that water oxidation is a key step in the photocatalytic reduction of CO_2. Indeed, during this process, holes (h^+) are oxidized with water molecules, leading to the formation of H^+ ions (Eq. 5–6). Subsequently, these ions react with CO_2 molecules and electrons to form valuable carbonaceous compounds such as CO and CH_4, as shown in Equations 3 and 4.[49] The reaction mechanism for hydrogen formation is provided in Equation 7.[50]
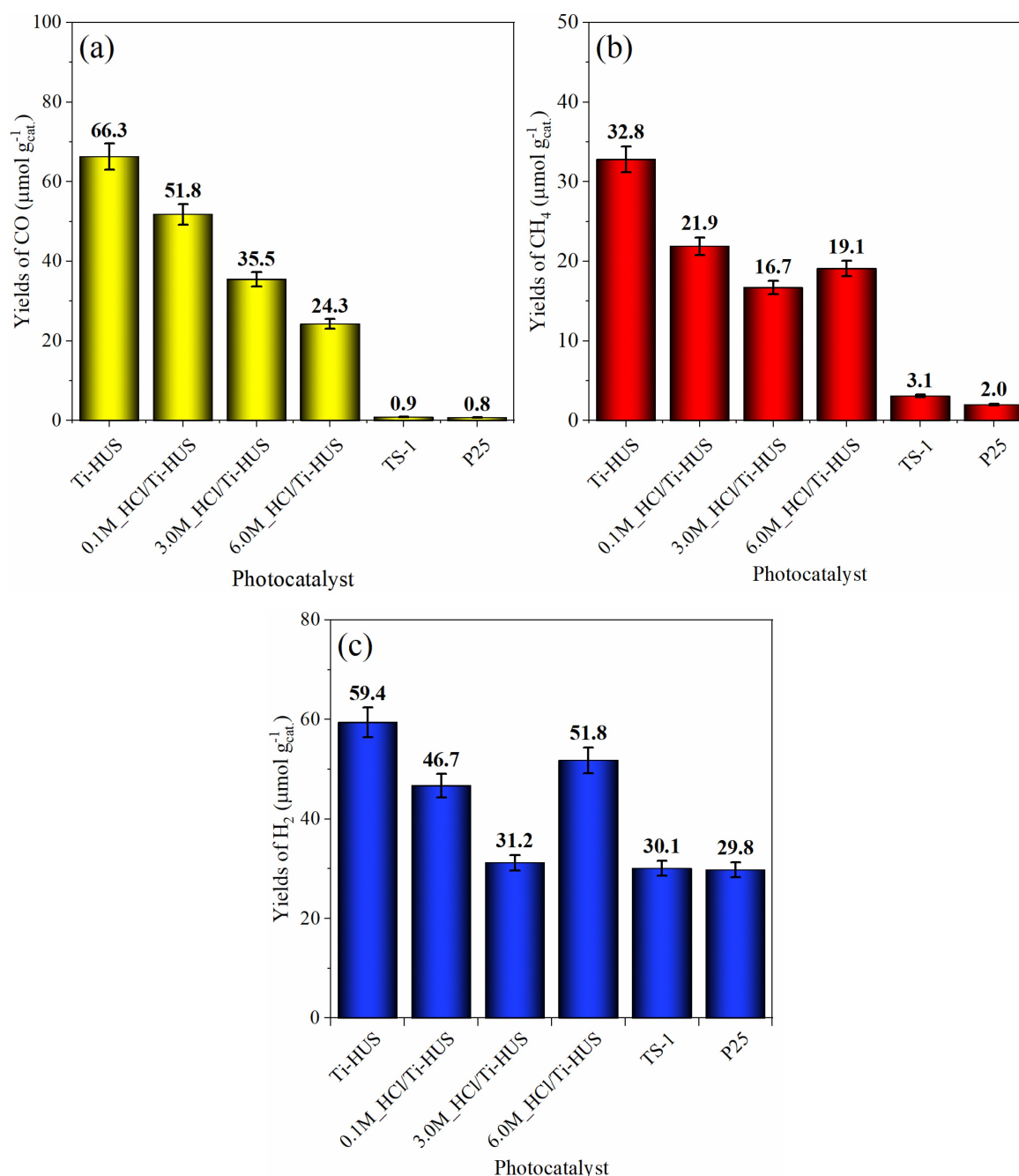
$$2H_2O + 4h^+ \rightarrow O_2 + 4H^+ \quad (5)$$

$$H_2O + h^+ \rightarrow \cdot OH + H^+ \quad (6)$$

$$2H^+ + 2e^- \rightarrow H_2 \quad (7)$$

ChemSusChem

Research Article
doi.org/10.1002/cssc.202400434

Chemistry Europe
European Chemical
Societies Publishing

Figure 6. Yields of a) CO, b) CH_4, and c) H_2 obtained from the photocatalytic reduction of CO_2 in the presence of investigated photocatalysts after 7 hours of UVC irradiation.

The investigated photocatalyst samples were measured at least 3 times, which means that the same batch (0.1 g of the photocatalyst sample with 100 ml of 0.2 M NaOH) was used each time and saturated with CO_2 again. The stability of the tested samples was verified by obtaining reproducible results in measurements of the photocatalytic reduction of CO_2. The measurement errors, as illustrated by the error bars in Figure 6, fell within a range of 5%.

Since it was suspected that the initial aqueous solution of 0.2 M NaOH etched the prepared photocatalyst samples, as is generally the case with titanosilicate-based photocatalysts, it should also be noted that CO_2 saturation of the reaction mixture at the beginning of the photocatalytic process leads to a rapid drop in pH from 12 to 7. In other words, as a result of CO_2 saturation, the conditions change from alkaline (pH = 12) to neutral (pH = 7), under which the stability of the photocatalysts is retained.[18]

Blank reactions were performed to ensure that the hydrocarbon was produced solely through the photoreduction of CO_2 and to eliminate any surrounding interference. The first blank (Blank test_1) was performed under UV illumination with the catalyst, an aqueous solution of NaOH without CO_2 saturation.

ChemSusChem

Research Article
doi.org/10.1002/cssc.202400434

Chemistry
Europe
European Chemical
Societies Publishing

The second blank (Blank test_2) was carried out with the catalyst, an aqueous solution of NaOH without CO_2 saturation and without UV illumination (under dark conditions), and the third (Blank test_3) was UV illuminated with the catalyst, deionized water without CO_2 saturation (Figure S6). In all cases, only CO_2 naturally absorbed from the air was present.[27] The obtained results confirmed that CO and CH_4 products arise from the photocatalytic reduction of CO_2 carried out in the presence of the Ti-HUS photocatalyst.

Since the photocatalytic reduction of CO_2 to CH_4 and CO represents a competitive reaction against the water splitting associated with hydrogen formation, the selectivity for the photocatalytic CO_2 reduction was calculated using Equation 2.

The calculated percentual proportions of the CH_4 and CO yields along with the selectivity values after 7 hours of irradiation over the investigated photocatalyst samples are illustrated and compared in Figure 7.

The results depicted in Figure 7 indicate that the synthesized Ti-HUS-based materials exhibit higher selectivity for CO_2 reduction than the reference samples of titanosilicate TS-1 and commercial TiO_2 P25. Their selectivity to CO and CH_4 molecules was even the lowest among all the photocatalyst samples tested. However, these samples exhibit high H_2 yields because the majority of the generated electrons participate in the competitive water splitting reaction, as described in Equation 7. Consequently, this result in lower selectivity for the photocatalytic CO_2 reduction.

Detailed analysis of the results revealed a strong dependence of the efficiency of the photocatalytic CO_2 reduction process on the modulation of surface Ti amounts in the investigated Ti-HUS-based photocatalyst samples. This depend-

ence was demonstrated by finding correlations between the yields of the CO and CH_4 molecules evolved during the photocatalytic reduction of CO_2 and the calculated Si/Ti ratios. These ratios are crucial for understanding how surface structure influences photocatalytic performance. They were determined using EDX and XPS, which are preferred due to their effectiveness in revealing such structural details. As shown in Figure 8a–b, the yields of the detected CO and CH_4 products of the investigated photocatalyst samples decrease with increasing Si/Ti ratios, corresponding to the enhanced photocatalytic performance of the synthesized Ti-HUS-based photocatalyst samples. This observation underscores the suitability of applying Ti-HUS layered photocatalysts for the photocatalytic CO_2 reduction reaction compared to the sample of titanium silicate TS-1, whose CO and CH_4 yields were significantly lower. Nadeem et al.[51] also highlighted a strong dependence of Si/Ti ratio on the photocatalytic reduction of CO_2 process. In their work, they pointed out an increase in photocatalytic activity for CO_2 reduction, as indicated by rising methanol yields, with a decreasing Si/Ti ratio in Ti-MCM-48 materials.

The above facts are also consistent with the detailed XPS analysis of the investigated samples, which reveals the exact amounts of Ti and Si elements on the surface of the Ti-HUS samples. Based on the results, it can be concluded that the higher yields of carbonaceous products (CO, CH_4) are linked to the elevated immobilized Ti (Figure 8c), whose atoms participating in the photocatalytic CO_2 reduction process. This claim is also supported by Wenhui et al.,[52] who highlighted the enhanced photocatalytic reduction of CO_2 due to the increasing Ti content in the Ti-MCM-41 materials.

Conversely, the gradual increase in silicon content led to a decrease in photocatalytic efficiency, corresponding to a decrease in the yields of CO and CH_4 products (Figure 8d).

Additionally, as demonstrated by UV-Vis DRS analysis, the limited light absorption ability in the UV region of the light spectra associated with a gradual decrease in absorbance in the wavelength range between 200 and 370 nm (Figure S7), along with the low distribution of Ti active sites on the surface of the TS-1 sample (Figure 9 a), should not be overlooked. These factors play a vital role in the low photocatalytic performance of the reference TS-1 sample.[53–55] On the other hand, as shown in Figure 9b, the distribution of immobilized Ti active sites on the surface of the layered Ti-HUS sample is significantly higher compared to that of the TS-1 sample. This observation plays another crucial role in the superior photocatalytic performance of the Ti-HUS sample, as the photocatalytic process primarily occurs on the surface of photocatalysts.

The photocatalytic activity for a CO_2 reduction of the synthesized Ti-HUS material samples was compared not only with the photocatalytic efficiency of the reference sample TS-1, but also with the commercial TiO_2 photocatalyst P25, which represents a benchmark in the heterogeneous photocatalysis.[56] As shown in Figures 6a–b and 7, it can be summarized that both the photocatalytic activity and selectivity for the photocatalytic CO_2 reduction of the commercial TiO_2 P25 were significantly lower compared to the synthesized Ti-HUS samples. The primary factor contributing to the low photocatalytic
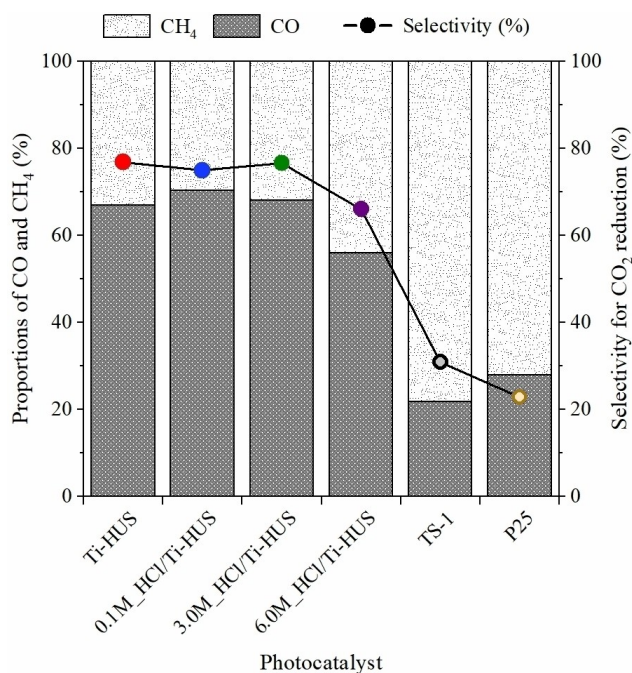

Figure 7. Proportions of CO and CH_4 yields (after 7 hours of UVC irradiation) and calculated percentage selectivity for the photocatalytic reduction of CO_2 over the investigated photocatalyst samples.

ChemSusChem

Research Article
doi.org/10.1002/cssc.202400434

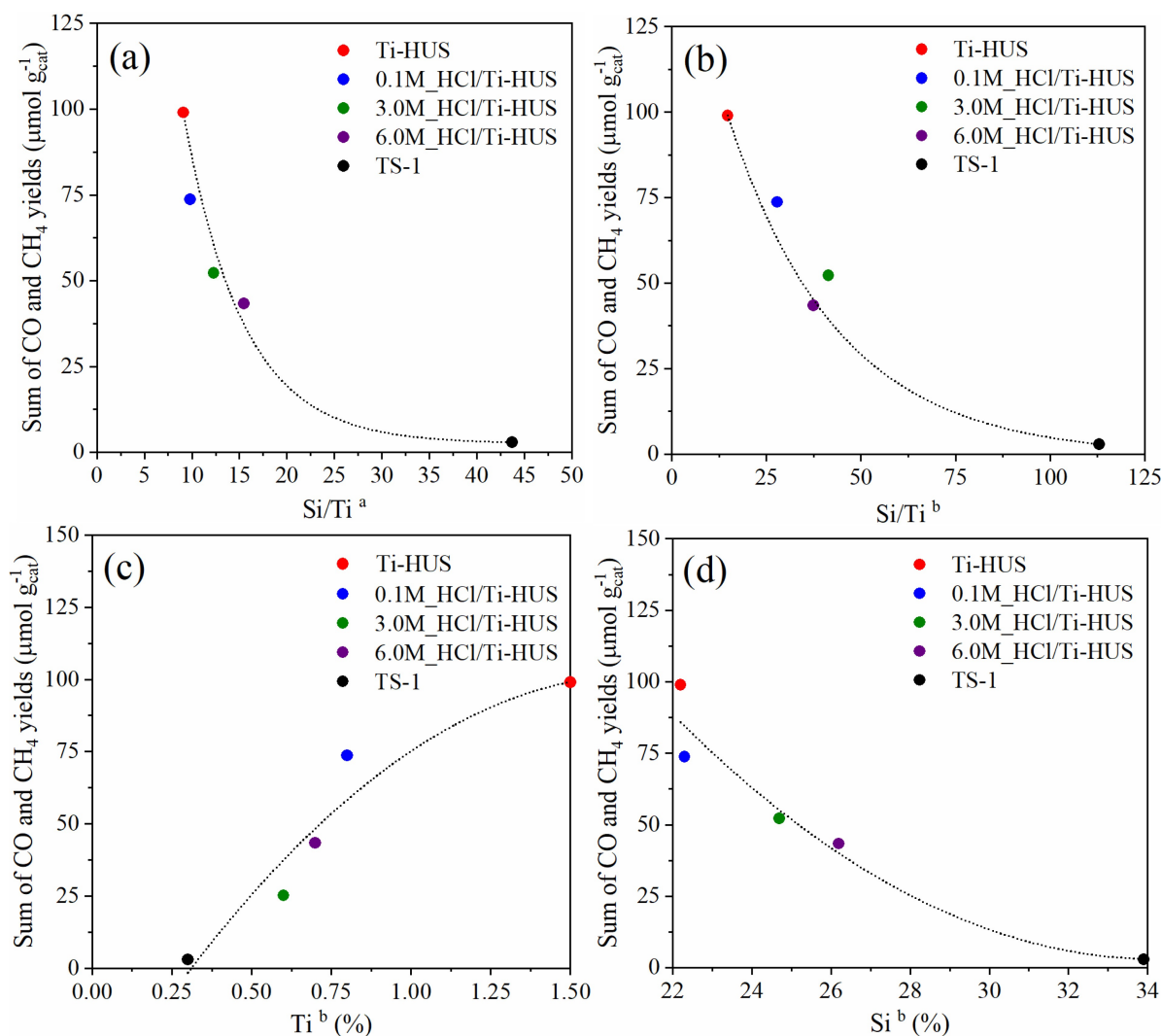**Chemistry Europe**
European Chemical
Societies Publishing

Figure 8. Correlations between the Si/Ti ratios determined by a) EDX, b) XPS, c) the amount of Ti, and d) Si and the resulting yields of CO and CH$_4$ as the primary products of the photocatalytic reduction of CO$_2$.

efficiency of the commercial TiO$_2$ P25 is probably the rapid charge carrier recombination, leading to a diminished efficiency of utilizing light energy for the photocatalytic process. This phenomenon represents one of the well-known drawbacks of the commercial TiO$_2$ P25.[57–59]

In order to propose a potential mechanism for the photocatalytic CO$_2$ reduction over Ti-HUS-based photocatalyst samples, it was crucial to elucidate the formation of H$_2$ during the experiments conducted. As stated previously, hydrogen represents the major product in the water splitting reaction (Eq. 7), which competes against CO$_2$ reduction. This finding is also consistent with the insights reported in the study by Edelmannová et al..[27] These facts contribute to understanding the origin of hydrogen produced during the photocatalytic CO$_2$ reduction tests. However, these observations do not provide any insight into the generation of H$_2$ over the Ti-HUS photocatalysts investigated in this work.

Subsequent analysis of the obtained results revealed a strong correlation between the rising yields of evolved H$_2$ and the decreasing amount of surface lattice oxygen species in the investigated photocatalysts (Figure 10a). The gradual decrease in the amount of surface lattice oxygen species can be attributed to the successful immobilization of gradually increasing amounts of isolated Ti species into the structure of the HUS-7 precursor, correlating with the rising yields of H$_2$, as shown in Figure 10b. This fact aligns with the findings of Dubnová et al.,[60] who demonstrated increased yields of H$_2$ with decreasing content of surface oxygen species resulting from doping of photocatalyst.

Through an understanding of the previously mentioned facts, along with finding a correlation between the increased yields of H$_2$ with the growing amount of immobilized Ti (as shown in Figure 10b), it is evident that the presence of Ti-based centers within the HUS-7 structure plays a crucial role in the formation of H$_2$ during the photocatalytic experiments. As further detailed, within these centers, transformations from the (Ti^{4+}–O^{2-}) state to the (Ti^{3+}–O$^-$)* photoinduced state occur due to UVC irradiation, which promotes the water splitting reaction
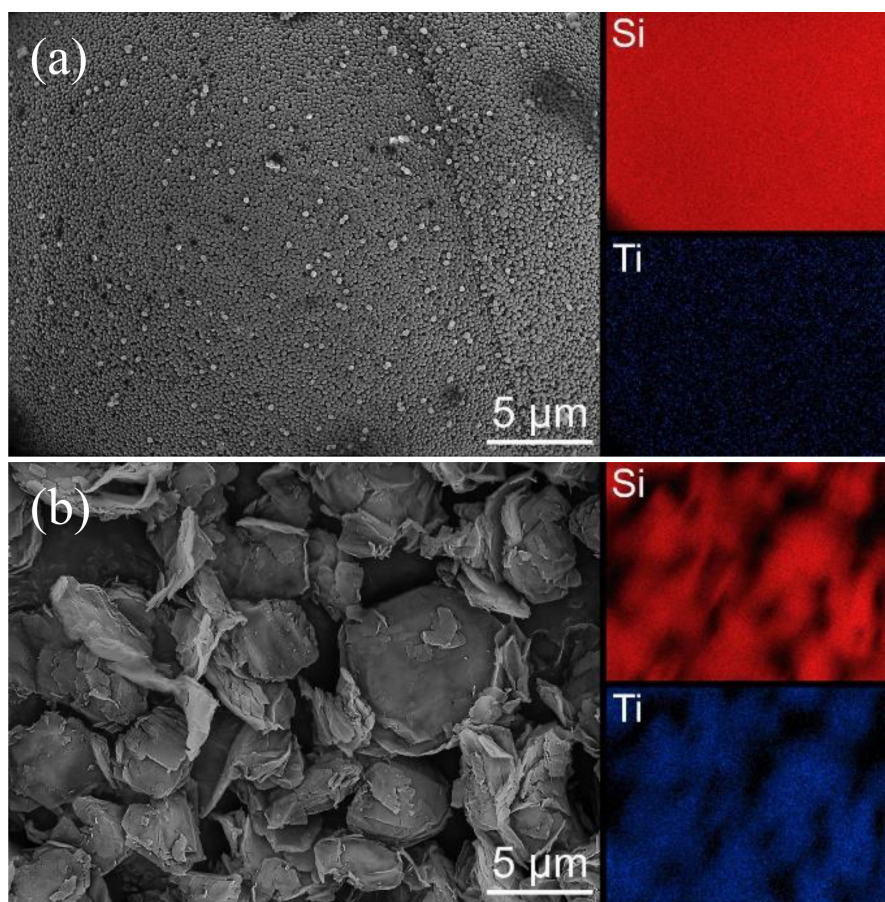
Figure 9. SEM-EDS images with the depicted Si and Ti maps for a) TS-1 and b) Ti-HUS samples.
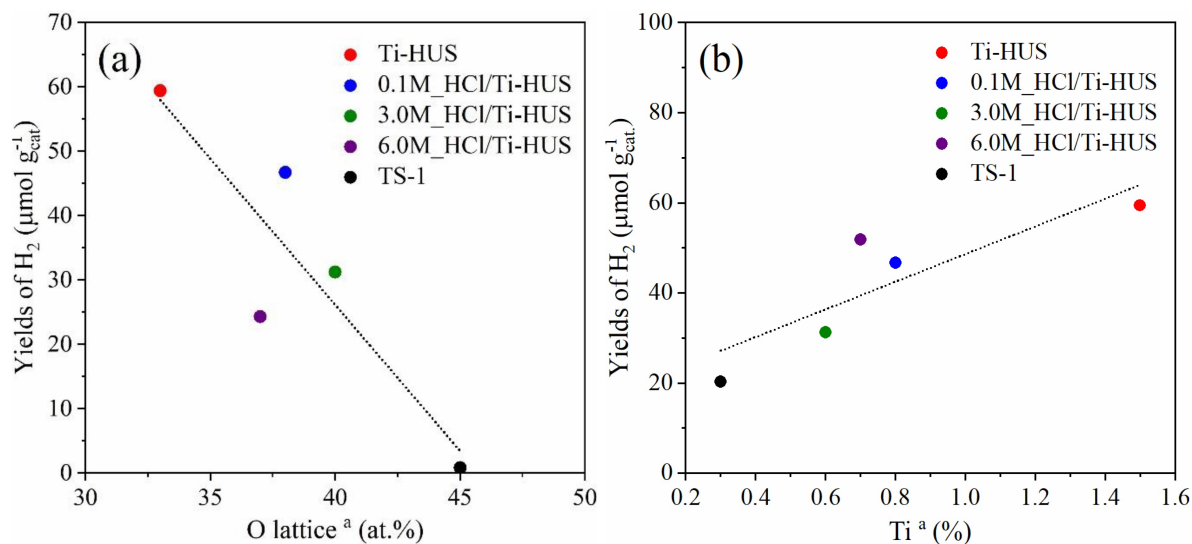

Figure 10. Correlations between H_2 yields evolved during the photocatalytic CO_2 reduction experiments and a) the quantity of lattice oxygen, and b) the amount of Ti species immobilized into the precursor HUS-7.

and leads to the generation of H_2.[61] Based on these findings, it can be concluded that an increase in the amount of immobilized Ti sites results in the formation of more photoinduced centers, thereby contributing to the improved photocatalytic

water splitting reaction and enhancing yields of H_2 as the primary product of this reaction.

The concentration of adsorbed OH groups emerges as another vital factor in assessing the photocatalytic performance

ChemSusChem

Research Article
doi.org/10.1002/cssc.202400434

Chemistry Europe
European Chemical
Societies Publishing

of Ti-HUS photocatalysts in the photocatalytic CO_2 reduction. This aspect is particularly relevant for the investigated Ti-HUS photocatalysts, where their presence and quantity were verified not only by FTIR, but also by XPS analysis. Indeed, in this case, the surface OH groups, along with the immobilized Ti species, likely acted as the active centers for the adsorption of reactants, thus influencing the selectivity in favor of higher yields of carbonaceous products.[33] Understanding these important facts also greatly facilitated the conception of the proposed mechanism described below.

As outlined in the previous paragraph, based on the reviewed literature and the obtained results, a possible mechanism has been formulated to elucidate the complex processes involved in the photocatalytic CO_2 reduction using the Ti-HUS-based photocatalysts. In the initial step, influenced by light irradiation, CO_2 and H_2O molecules react with the tetrahedrally coordinated Ti active centers. Subsequently, the so-called ligand to metal charge transfer (LMCT) process occurs, involving the transfer from the original $(Ti^{4+}-O^{2-})$ to the $(Ti^{3+}-O^-)^*$ photoexcited states.[62] The transfer of electrons from $(Ti^{3+}-O^-)^*$ to CO_2 leads to the fragmentation of the CO_2 molecule and the generation of intermediate products, particularly CO, which serves as both an intermediate and also a product of the photoreduction of CO_2. Moreover, hydrogen atoms and hydroxyl radicals, generated from the concurrent competitive water splitting reaction of H_2O molecules, engage in further reactions with carbon-based species derived from the reduction of CO_2 molecules and form valuable carbonaceous compounds, such as methane in this case.[33,63–66]

Hussain et al.[67] even successfully achieved the evolution of methanol (CH_3OH) by the photocatalytic CO_2 reduction over Ti-incorporated KIT-6 materials (Korea Advanced Institute of Science and Technology-6 silica) by a similar mechanism based on the carbene pathway.[64]

The above-mentioned facts also explain the lower photocatalytic activity of commercial TiO_2 P25 observed during the photocatalytic CO_2 reduction compared to the layered Ti-HUS-based samples, which demonstrate higher photocatalytic performance. Indeed, this photocatalyst not only suffers from well-known drawbacks related to its wide band gap (3.2 eV) and rapid charge carrier recombination, but also maintains stability upon exposure to UVC irradiation. However, in the case of the investigated layered samples based on Ti-HUS, UVC radiation induces a transition of immobilized Ti species from the original states $(Ti^{4+}-O^{2-})$ to photoexcited Ti^{3+}-based states $(Ti^{3+}-O^-)^*$, thereby significantly increasing the photocatalytic efficiency during photocatalytic reduction CO_2.

3. Conclusions

In conclusion, we have successfully synthesized titanium-immobilized layered HUS silicate (Ti-HUS) photocatalyst samples using a combined precipitation method. By subjecting the samples to acid treatment with varying concentrations of HCl (0.1, 3.0, and 6.0 mol dm^{-3}), we modulated the amount of immobilized isolated Ti species. Our investigation demonstrated the efficacy of these Ti-HUS-based samples in the photocatalytic CO_2 reduction process, showcasing superior activity and selectivity compared to widely studied reference samples, TS-1 and commercial TiO_2 P25. Analysis revealed a direct relationship between increased carbonaceous product yields, elevated Ti species immobilization, and decreased Si content. Additionally, we observed the competitive formation of H_2 during photocatalytic water splitting, correlated with decreasing surface lattice oxygen concentration and increasing isolated Ti species content. Furthermore, we propose a mechanism elucidating the role of isolated Ti species and surface OH groups in enhancing selectivity and yield of carbonaceous products during CO_2 reduction. Our findings underscore the potential of HUS-7-based materials as promising candidates for CO_2 photoreduction, suggesting avenues for future research in this field.

Conflict of Interests

The authors declare no conflict of interest.

Data Availability Statement

The data that support the findings of this study are available from the corresponding author upon reasonable request.

[1] X. Ren, M. Gao, Y. Zhang, Z. Zhang, X. Cao, B. Wang, X. Wang, *Appl. Catal. B* **2020**, *274*, 119063.
[2] N.-N. Vu, S. Kaliaguine, T.-O. Do, *Adv. Funct. Mater.* **2019**, *29*, 1901825.
[3] H. Shen, T. Peppel, J. Strunk, Z. Sun, *Solar RRL* **2020**, *4*, 1900546.

ChemSusChem

Research Article
doi.org/10.1002/cssc.202400434

Chemistry
Europe
European Chemical
Societies Publishing

[4] H. Pan, M. D. Heagy, *Nanomaterials* **2020**, *10*.

[5] P. Madhusudan, R. Shi, S. Xiang, M. Jin, B. N. Chandrashekar, J. Wang, W. Wang, O. Peng, A. Amini, C. Cheng, *Appl. Catal. B* **2021**, *282*, 119600.

[6] A. Bathla, J. Lee, S. A. Younis, K.-H. Kim, *Mater. Today Chem.* **2022**, *24*, 100870.

[7] W. A. Thompson, E. Sanchez Fernandez, M. M. Maroto-Valer, *ACS Sustainable Chem. Eng.* **2020**, *8*, 4677–4692.

[8] Q.-s. Wang, Y.-c. Yuan, C.-f. Li, Z.-r. Zhang, C. Xia, W.-g. Pan, R.-t. Guo, *Small* **2023**, 2301892

[9] W. Wang, L. Wang, W. Su, Y. Xing, *J. CO2 Util.* **2022**, *61*, 102056.

[10] D. Ješić, D. Lašič Jurković, A. Pohar, L. Suhadolnik, B. Likozar, *Chem. Eng. J.* **2021**, *407*, 126799.

[11] Z. Shang, X. Feng, G. Chen, R. Qin, Y. Han, *Small* **2023**, 2304975

[12] T. Zhang, X. Han, N. T. Nguyen, L. Yang, X. Zhou, *Chin. J. Catal.* **2022**, *43*, 2500–2529.

[13] Z. Sun, X. Huang, G. Zhang, *J. Cleaner Prod.* **2022**, *381*, 135156.

[14] T. Fawzi, S. Rani, S. C. Roy, H. Lee, *Int. J. Mol. Sci.* **2022**, *23*, 8143.

[15] N. Li, W. Zhang, D. Wang, G. Li, Y. Zhao, *Chem. Asian J.* **2022**, *17*, e202200822.

[16] S. Ferdov, B. Shivachev, N. Drenchev, K. Hadjiivanov, S. Simova, R. Titorenkova, N. Petrova, M. Tarassov, R. Nikolova, *Microporous Mesoporous Mater.* **2024**, *363*, 112829.

[17] N. Tsunoji, M. V. Opanasenko, M. Kubů, J. Čejka, H. Nishida, S. Hayakawa, Y. Ide, M. Sadakane, T. Sano, *ChemCatChem.* **2018**, *10*, 2536–2540.

[18] B. T. Barrocas, J. Přech, M. Filip Edelmannová, E. Szaniawska, K. Kočí, J. Čejka, *Applied Materials Today* **2022**, *26*, 101392.

[19] Y. Wang, H. Yang, Y. Zuo, D. Tian, G. Hou, Y. Su, Z. Feng, X. Guo, C. Li, *Appl. Catal. B* **2023**, *325*, 122396.

[20] A. Guntida, B. Jongsomjit, P. Praserthdam, P. Praserthdam, *Fuel* **2022**, *314*, 122736.

[21] M. Signorile, L. Braglia, V. Crocellà, P. Torelli, E. Groppo, G. Ricchiardi, S. Bordiga, F. Bonino, *Angew. Chem. Int. Ed.* **2020**, *59*, 18145–18150.

[22] N. Tsunoji, H. Nishida, Y. Ide, K. Komaguchi, S. Hayakawa, Y. Yagenji, M. Sadakane, T. Sano, *ACS Catal.* **2019**, *9*, 5742–5751.

[23] N. Tsunoji, Y. Ide, Y. Yagenji, M. Sadakane, T. Sano, *ACS Appl. Mater. Interfaces* **2014**, *6*, 4616–4621.

[24] O. H. Weiergräber, M. Schwarten, B. Strodel, D. Willbold in *Chapter Eight - Investigating Structure and Dynamics of Atg8 Family Proteins, Vol. 587* (Eds.: L. Galluzzi, J. M. Bravo-San Pedro, G. Kroemer), Academic Press, **2017**, pp.115–142.

[25] T. Wu, X. Zhu, Z. Xing, S. Mou, C. Li, Y. Qiao, Q. Liu, Y. Luo, X. Shi, Y. Zhang, X. Sun, X. Wu, Z. Zhu, S. Xing, C. Mou, Y. Li, Q. Qiao, Y. Liu, X. Zhang, X. Shi, *NitrogenR eduction Reaction Greatly Improving Electrochemical N2 Reduction over TiO2 Nanoparticles by IronDoping*, **2019**.

[26] M. C. Biesinger, L. W. M. Lau, A. R. Gerson, R. S. C. Smart, *Appl. Surf. Sci.* **2010**, *257*, 887–898.

[27] M. Filip Edelmannová, M. Reli, P. Nadrah, N. Rozman, R. Ricka, A. Sever Škapin, M. Nosan, U. Lavrenčič Štangar, K. Kočí, *Catal. Today* **2023**, *413–415*, 113944.

[28] G. Bancroft, H. Nesbitt, R. Ho, D. Shaw, J. Tse, M. Biesinger, *Phys. Rev. B* **2009**, *80*.

[29] C.-Q. Liu, L. Cui, Y. Liu, Z.-R. Shen, P. Xie, R.-B. Zhang, *Liq. Cryst.* **2000**, *27*, 907–916.

[30] M. Mecozzi, M. Pietroletti, M. Scarpiniti, R. Acquistucci, M. E. Conti, *Environ. Monit. Assess.* **2011**, *184*, 6025–6036.

[31] F. Ferati in *Structural Information from Ratio Bands in the FTIR Spectra of Long Chain and Branched Alkanes in Petrodiesel Samples*, Vol. (Ed. Eds.: Editor), City, **2020**, 1140–1143.

[32] D. Widjonarko, I. Kartini, *Indonesian Journal of Chemistry* **2014**, *14*, 143–151.

[33] P. Akhter, M. Hussain, G. Saracco, N. Russo, *Nanoscale Res. Lett.* **2014**, *9*, 158.

[34] G. Wallidge, R. Anderson, G. Mountjoy, D. Pickup, P. Gunawidjaja, R. Newport, M. Smith, *J. Mater. Sci.* **2004**, *39*.

[35] Y. Lai, L. Jin, J. Hang, X. Sun, L. Shi, *J. Coat. Technol. Res.* **2015**, *12*, 1185–1192.

[36] G. Lv, S. Deng, Y. Zhai, Z. Zhu, H. Li, F. Wang, X. Zhang, *Appl. Catal. A* **2018**, *567*, 28–35.

[37] H. Tada, Q. Jin, H. Nishijima, H. Yamamoto, M. Fujishima, S. Okuoka, T. Hattori, Y. Sumida, H. Kobayashi, *Angew. Chem. Int. Ed. Engl.* **2011**, *50*, 3501–3505.

[38] C. Stienen, D. Rogalla, O. Prymak, G. Bendt, *Eur. J. Inorg. Chem.* **2021**, *2021*, 4298–4306.

[39] N. Blommaerts, N. Hoeven, D. Arenas Esteban, R. Campos, M. Mertens, R. Borah, A. Glisenti, K. De Wael, S. Bals, S. Lenaerts, S. W. Verbruggen, P. Cool, *Chem. Eng. J.* **2021**, *410*, 128234.

[40] V. A. de la Peña O'Shea, M. Capel-Sanchez, G. Blanco-Brieva, J. M. Campos-Martin, J. L. Fierro, *Angew. Chem. Int. Ed. Engl.* **2003**, *42*, 5851–5854.

[41] A. Zandonà, E. Chesneau, G. Helsch, A. Canizarès, J. Deubener, V. Montouillout, F. Fayon, M. Allix, *J. Non-Cryst. Solids* **2022**, *598*, 121967.

[42] B. C. Ledesma, O. A. Anunziata, A. R. Beltramone, *Appl. Catal. B* **2016**, *192*, 220–233.

[43] L. A. Farrow, E. M. Vogel, *J. Non-Cryst. Solids* **1992**, *143*, 59–64.

[44] Y. Chen, X. Luo, Y. Luo, P. Xu, J. He, L. Jiang, J. Li, Z. Yan, J. Wang, *Nanomaterials.* **2019**, *9*, 698.

[45] F. Garbassi, L. Balducci, *Microporous Mesoporous Mater.* **2001**, *47*, 51–59.

[46] I. Petrik, G. V. Krylova, O. O. Kelyp, L. Lutsenko, N. P. Smirnova, L. Oleksenko, *Himia, Fizika ta Tehnologia Poverhni.* **2015**, *6*, 179–189.

[47] B. Kanjilal, A. Masoumi, I. Noshadi in *Chapter 11 - Photocatalytic process for syngas production, Vol. 1* (Eds.: M. R. Rahimpour, M. A. Makarem, M. Meshksar), Elsevier, **2023**, pp.261–290.

[48] R. Ricka, A. Wanag, E. Kusiak-Nejman, D. Moszyński, M. Edelmannová, M. Reli, Z. Baďura, G. Zoppellaro, R. Zboril, A. Morawski, K. Kočí, *J. CO2 Util.* **2024**, *80*, 102701.

[49] M. Reli, P. Nadrah, M. Filip Edelmannová, R. Ricka, A. Sever Škapin, U. Lavrenčič Štangar, K. Kočí, *Mater. Sci. Semicond. Process.* **2024**, *169*, 107927.

[50] M. Tasbihi, M. Schwarze, R. Schomäcker in *Photocatalytic CO₂ Reduction and Beyond, Vol.*, **2021**, pp.287–302.

[51] S. Nadeem, A. Mumtaz, M. Mumtaz, M. I. Abdul Mutalib, M. S. Shaharun, B. Abdullah, *J. Mol. Liq.* **2018**, *272*, 656–667.

[52] W. Jia, T. Liu, Q. Li, J. Yang, *Catal. Today* **2019**, *335*, 221–227.

[53] J. Li, X. Pei, Z. Wang, Y. Li, G. Zhang, *Appl. Surf. Sci.* **2022**, *605*, 154632.

[54] Q. Wang, Z. Fang, X. Zhao, C. Dong, Y. Li, C. Guo, Q. Liu, F. Song, W. Zhang, *ACS Appl. Mater. Interfaces* **2021**, *13*, 59855–59866.

[55] C. Perdomo, N. T. Nguyen, *Curr. Opin. Colloid Interface Sci.* **2022**, *61*, 101625.

[56] D. Zanardo, G. Forghieri, S. Tieuli, E. Ghedini, F. Menegazzo, A. Di Michele, G. Cruciani, M. Signoretto, *Catal. Today* **2022**, *387*, 54–60.

[57] D. Eakhmawaty Eddy, S. Ishmah, M. D. Permana, M. Firdaus, I. Rahayu, Y. el-badry, E. Hussein, Z. El-Bahy, *Appl. Sci.* **2021**, *11*, 9033.

[58] K. Wang, Z. Wei, C. Colbeau-Justin, A. Nitta, E. Kowalska, *Surfaces* **2022**, *31*, 102057.

[59] G. Liao, X. Tao, B. Fang, *Matter.* **2022**, *5*, 377–379.

[60] L. Dubnová, M. Zvolská, M. Edelmannová, L. Matějová, M. Reli, H. Drobná, P. Kuśtrowski, K. Kočí, L. Čapek, *Appl. Surf. Sci.* **2019**, *469*, 879–886.

[61] X. Zhang, Z. Li, B. Zeng, C. Li, H. Han, *J. Energy Chem.* **2022**, *70*, 388–393.

[62] G. Petcu, E. M. Anghel, I. Atkinson, D. C. Culita, N. G. Apostol, A. Kuncser, F. Papa, A. Băran, J.-L. Blin, V. Parvulescu in *Composite Photocatalysts with Fe, Co, Ni Oxides on Supports with Tetracoordinated Ti Embedded into Aluminosilicate Gel during Zeolite Y Synthesis*, Vol. (Ed.Eds.: Editor), Preprints, City, **2024**, 129

[63] K. Mori, H. Yamashita, M. Anpo, *RSC Adv.* **2012**, *2*, 3165–3172.

[64] J. Zhang, J. Jiang, Y. Lei, H. Liu, X. Tang, H. Yi, X. Huang, S. Zhao, Y. Zhou, F. Gao, *Sep. Purif. Technol.* **2024**, *328*, 125056.

[65] M. Song, X. Song, X. Liu, W. Zhou, P. Huo, *Chin. J. Catal.* **2023**, *51*, 180–192.

[66] W. Cai, Z. Qian, C. Hu, W. Zheng, L. Luo, Y. Zhao, *Chem. Eng. J.* **2024**, *479*, 147718.

[67] M. Hussain, P. Akhter, N. Russo, G. Saracco, *Chem. Eng. J.* **2015**, *278*, 279–292.